Framework for predicting noise-power-distance curves for novel aircraft designs

Synodinos, AP, Self, RH and Torija Martinez, AJ

http://dx.doi.org/10.2514/1.C034466

A framework for predicting Noise-Power-Distance curves for novel aircraft designs

Journal:	*Journal of Aircraft*
Manuscript ID	2017-03-C034466.R1
Manuscript Type:	Full Paper
Date Submitted by the Author:	n/a
Complete List of Authors:	Synodinos, Athanasios; University of Southampton, Institute of Sound and Vibration Research Self, Rodney; University of Southampton, Institute of Sound and Vibration Research Torija, Antonio; University of Southampton, Institute of Sound and Vibration Research
Subject Index Category:	02200 Noise < 00000 AIRCRAFT TECHNOLOGY, CONVENTIONAL, STOL/VTOL
Note: The following files were submitted by the author along with the article. You may review these files online, if you wish. Acceptance for publication will be based solely on the content of the article.	
2017-03-C034466.zip	

A framework for predicting Noise-Power-Distance curves for novel aircraft designs

Athanasios P. Synodinos[a] and Rod H. Self[b] and Antonio J. Torija[c]
University of Southampton, Southampton, England SO17 1BJ, United Kingdom

Along with flight profiles, Noise-Power-Distance (NPD) curves are the key input variable for computing noise exposure contour maps around airports. With the development of novel aircraft designs (incorporating noise reduction technologies) and new noise abatement procedures, NPD datasets will be required for assessing their potential benefit in terms of noise reduction around airports. NPD curves are derived from aircraft flyover noise measurements taken for a range of aircraft configurations and engine power settings. Clearly then, empirical NPD curves will be unavailable for novel aircraft designs and novel operations. This paper presents a generic framework for computationally generating NPD curves for novel aircraft and situations. The new framework derives computationally the NPD noise levels that are normally derived experimentally, by estimating noise level variations arising from technological and operational changes with respect to a baseline scenario, where the noise levels are known, or otherwise estimated. The framework is independent of specific prediction methods and can use any potential new model for existing or new noise sources. The paper demonstrates the methodology of the framework, discusses its benefits and illustrates its applicability by deriving NPD curves for an unconventional approach operation and for a future concept blended-wing-body (BWB) aircraft.

[a] PhD student, Institute of Sound and Vibration Research, a.synodinos@soton.ac.uk.
[b] Professor, Institute of Sound and Vibration Research.
[c] Senior research fellow, Institute of Sound and Vibration Research.

Nomenclature

A = cross sectional area

C = constant related to ambient conditions

D = directivity

d = test slant distance

F = thrust

j = engine power setting

$L_{A,mx}$ = maximum A-weighted sound pressure level

L_w = sound power level

m = mass flow rate

R = distance from aircraft

r = other slant distances i.e. different from d

t = time

V = velocity

W = acoustic power

δ = flap deflection angle

ρ = density

θ = polar angle

ϕ = azimuthal angle

Subscripts

0 = baseline value

ac = aircraft

b = bypass stream of turbofan engine

c = core stream of turbofan engine

e = effective

f = fan

κ = fan noise component

G = gross

j = jet

N = net

ref = reference value

s = noise source

τ = airframe component

I. Introduction

It is generally recognised that new noise impact mitigation strategies must be introduced to compensate for the forecast increase in air transportation demand [1, 2]. Mitigation strategies involve adopting, among others, new technologies, re-shaped operational procedures and refurbished government policies. Different noise metrics are used to describe these strategies and to support the associated decision making. For instance, aircraft manufacturers need to comply with the ICAO certification levels [3], as measured in EPNdB. In contrast, authorities aiming at minimising community impacts, i.e. reducing the population exposed to specific aircraft noise levels at particular geographic areas over a period of time, track and report the noise impact in the form of noise exposure contour maps. For instance, the UK's Civil Aviation Authority presents yearly noise exposure contours around London airports [4], on behalf of the Department for Transport.

Noise exposure contour maps are essential to many aviation legislators and planners worldwide for communicating aircraft noise levels in the vicinity of airports, in a graphical and comprehensible way to the non-expert. They are produced (typically yearly) according to the standard ECAC method [5], which is the method normally adopted by airport noise evaluation software, such as the FAA's Integrated Noise Model (INM)[6] and the Aviation Environmental Design Tool (AEDT) [7]. The fundamental input to that ECAC method is the Noise-Power-Distance curves (NPDs).

NPDs development starts from experimentally acquired aircraft noise levels (referred to in this paper as initial levels). Due to the fact that experimental measurements are costly, time consuming and often difficult to organise, it is practically impossible to conduct tests for any possible aircraft configuration. As a result, several similar aircraft are assigned the same NPDs [5]. Whereas obviously, it is unfeasible to produce NPDs for future aircraft designs. Consequently, noise contour maps construction is currently restricted to scenarios involving only existing aircraft and conventional operations. This contaminates forecast airport noise data, impeding future planning and possibly leading to misleading noise abatement operational procedures.

This paper presents a new framework for producing NPD curves, which is purely computational and bypasses the dependence on measurements, provided the existence of a baseline scenario, for which noise levels are known (e.g. from sources like the ICAO Aircraft Noise and Performance (ANP)

Database [8]). The difference between the proposed framework and the standard SAE AIR1845 NPD development procedure [9] is that the former estimates initial noise levels rather than experimentally acquiring them. Estimated initial levels are then extrapolated to the other NPD distances through the standard procedure in [9]. An important advantage of the framework is that it uses inputs and noise prediction methods for individual aircraft noise sources that are publicly available. Also, it is not bound to particular noise prediction methods and can use any potential new ones for existing and new noise sources.

Starting from a baseline scenario, the framework presented in this paper is able to generate NPDs for imminent and future aircraft designs, as well as for contemporary operations. Therefore, it can be coupled with both high-fidelity (INM [6], ANCON[10]) and simplified (RANE [11]) airport noise models and used by the aviation industry to contribute to decision making on which future technology platforms is likely to achieve the highest reduction of noise impact around airports.

II. NPD curves

NPD curves provide the relationship between the sound-level of a given aircraft at a reference flight speed and atmosphere, and the slant distance from the flight path, for a certain aircraft configuration (i.e. flap setting, etc.) and a number of engine power settings. The procedure to derive NPDs is analytically described in the SAE AIR1845 document [9] and briefly presented in Appendix C. NPD curves for most existing aircraft and conventional operations are publicly accessible from the ICAO ANP Database [8] that additionally provides aircraft performance data.

Each aircraft is assigned different NPDs for takeoff and landing. This is because aircraft configuration (i.e. flap setting, thrust setting, etc.) that varies between operations, determines the noise emitted from the aircraft [12]. In NPDs, the engine power parameter represents the net thrust per engine. For a given aircraft model and operation, the NPD engine power values are established with respect to its engine certification ratings [5]. The noise levels are provided at ten standard slant distances in different single event noise metrics, including Sound Exposure Level (SEL) and $L_{A,mx}$. As an example, Fig. 1 shows the SEL NPD curves for an Airbus A330-301 during take-off. Each curve describes different engine power settings.

The standard SAE AIR1845 procedure for developing NPD curves for a certain aircraft type

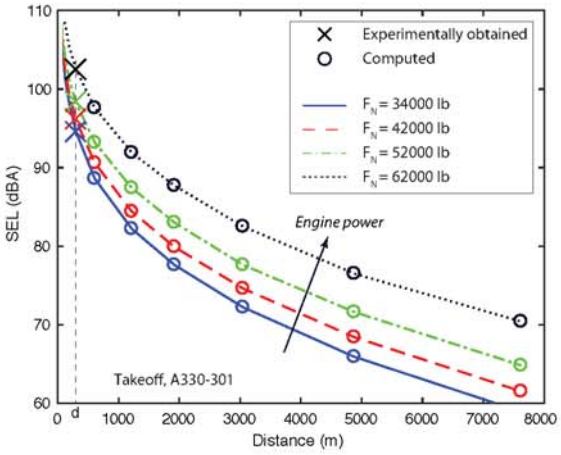

Fig. 1 SEL NPD curves for the A330-301 at takeoff. F_N represents net thrust per engine. Data obtained from [8].

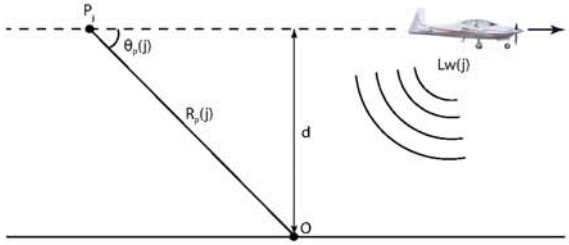

Fig. 2 Schematic representation of the typical test flyover for obtaining NPD data. Symbol O indicates the microphone position. L_w and P_j represent the aircraft PWL and the location of $L_{A,mx}$ occurrence respectively, when the aircraft operates at engine power setting j.

and operation principally comprises of an experimental and a computational part. More specifically, flyover noise measurements at locations directly under the flight path are first conducted at a certain slant distance (height) for each NPD engine power setting. With reference to Fig. 1, this procedure yields the SEL values corresponding to the NPD points marked with a cross. Then, accounting for effects of spherical wave spreading, atmospheric absorption as well as for differences on the effective duration, these experimentally measured noise levels are propagated to the other standard NPD distances (ascending up to 25,000 ft), yielding points marked with a circle in Fig. 1.

Figure 2 illustrates the experimental flyover for NPDs development. The test aircraft flies at constant height d at a fixed engine power setting j, generating sound power level (PWL), $Lw(j)$.

Symbol O indicates the microphone position. Point $P(j)$ and polar angle $\theta_P(j)$ represent the location where $L_{A,mx}$ occurs, which is at distance R_P away from the microphone. The objective of the experiment is to measure the $L_{A,mx}$ and SEL of the test flyover, for a set of pre-defined engine power settings j. The framework described in this paper has been developed to compute NPDs without the need of conducting noise measurements, which will allow for obtaining NPDs for future aircraft concepts.

III. The framework architecture

A. Overview

Aircraft noise consists of the contributions from engine noise sources (e.g. noise from the fan, the jet, etc.) and airframe noise sources (e.g. noise from landing gear, flaps, etc.). So, with N being the total number of noise sources, the aircraft PWL at engine power setting j can be decomposed into the contributions Lw_s from each source s, so that

$$Lw(j) = 10 \log \left[\sum_{s=1}^{N} 10^{\frac{Lw_s(j)}{10}} \right] . \tag{1}$$

In the developed framework, the aircraft is considered to be a lumped noise source, where all noise sources are collocated at its centre of gravity. Under this consideration, the $L_{A,mx}$ is calculated with

$$L_{A,mx}(d, j) = Lw(j) + 10 \log \left[\frac{D(\theta_P, j)}{R_P(j)^2} \right] + C \, , \tag{2}$$

where

$$C = \frac{\rho c}{4 \pi p_{ref}^2} \tag{3}$$

is a constant related to ambient conditions. The lumped aircraft directivity D is a function of the Lw_s and directivity, D_s of each source. Considering only the polar angle, since measurements are made directly under the flight path (so azimuthal angle $\phi = 0$), it can be shown that

$$D(\theta, j) = \frac{\sum_{s=1}^{N} \left[10^{\frac{Lw_s(j)}{10}} D_s(\theta) \right]}{\left[\sum_{s=1}^{N} 10^{\frac{Lw_s(j)}{10}} \right]} . \tag{4}$$

Equations (1 – 4) suggest that the sought $L_{A,mx}(j)$ is ultimately a function of the noise and directivity of each individual aircraft noise source. Several dedicated, publicly available semi-empirical methods exist for the noise prediction of individual aircraft noise sources, such as Heidmann [19] for

fan noise and Stone [22] for jet noise. But these require numerous design and operational inputs, some of which are proprietary to manufacturers. So despite the existence of these methods, accurate forecasts for general use are hard to achieve.

Assuming that semi-empirical method M predicts the noise level Lw_s of source s and that Lw_s is a function of parameters $\zeta_0, \xi_0, ..., \psi_0$; then

$$Lw_s = f(\zeta_0, \xi_0, ..., \psi_0)\,. \tag{5}$$

If parameters ζ_0, ψ_0 become ζ, ψ as a result of implicating a new scenario, while ξ_0 remains fixed, the noise level becomes

$$Lw'_s = f(\zeta, \xi_0, ..., \psi)\,. \tag{6}$$

While it is hard to obtain accurate results for Lw'_s which again, requires knowledge of numerous parameters, it is feasible to calculate, or at least obtain good estimates of the noise level change

$$\Delta Lw_s = 10\log\left[\frac{f(\zeta, \xi_0, ..., \psi)}{f(\zeta_0, \xi_0, ..., \psi_0)}\right] \tag{7}$$

between these two conditions. This is because knowledge of fixed parameters (e.g. geometry information) becomes redundant when estimating incremental changes. In fact, it is shown later in Section IV B that ΔLw_s is a function of just a few parameters that can be estimated based on publicly available information.

The framework exploits this substantial advantage of working in terms of changes rather than with absolute values. Hence, it considers that a new scenario evolves from a baseline scenario, which has been subjected to aircraft technology and/or operational changes. These changes translate into noise level variations ΔLw_s of each aircraft noise source and hence, to a noise level change ΔLw for the whole aircraft.

For a given engine power setting j, level change $\Delta Lw(j)$ induces a $L_{A,mx}$ difference $\Delta L_{A,mx}(d, j)$ at slant distance d. From Eq. 2, it can be shown that

$$\Delta L_{A,mx}(d, j) = \Delta Lw(j) + 10\log\frac{D(\theta_P)}{D_0(\theta_{P0})} + 20\log\frac{\sin\theta_P}{\sin\theta_{P0}}\,, \tag{8}$$

where parameters representing the baseline scenario have the subscript 0.

Figure 3 demonstrates that $\Delta L_{A,mx}(d, j)$ can be added to an experimentally-known baseline NPD level $L_{A,mx,0}(d, j)$ (marked with a cross) to yield the aircraft $L_{A,mx}$ reflecting to the new

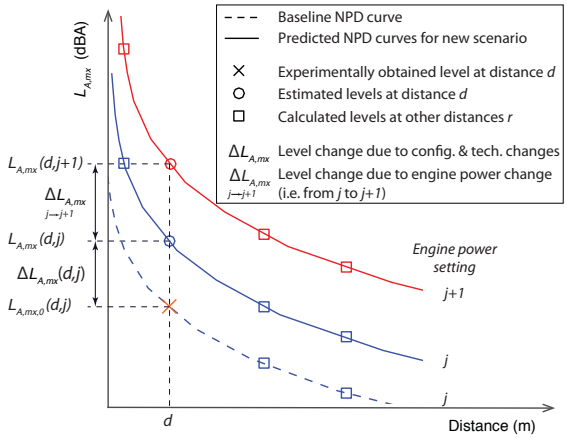

Fig. 3 Schematic representation of deriving NPD curves for a new scenario starting from a point on a baseline NPD curve.

scenario at the same power setting and slant distance, so

$$L_{A,mx}(d,j) = L_{A,mx,0}(d,j) + \Delta L_{A,mx}(d,j)\,. \tag{9}$$

The levels at the remaining engine power settings at the same distance d are obtained by adding the noise level variation resulting from changing the engine power setting from j to $j+1$, so that

$$L_{A,mx}(d,j+1) = L_{A,mx}(d,j) + \Delta L_{A,mx}(j \to j+1)\,. \tag{10}$$

Once the maximum levels at distance d, i.e. $L_{A,mx}(d)$ are estimated for all NPD engine power settings, they are propagated to the remaining NPD distances r through the SAE AIR1845 computational step (described thoroughly in reference [9]) in order to obtain $L_{A,mx}(r)$ and develop the complete $L_{A,mx}$ NPD curves.

Then, SAE AIR 1845 [9] computes the SEL at NPD distances r with

$$\mathrm{SEL}(r) = \mathrm{SEL}(d) + [L_{A,mx}(r) - L_{A,mx}(d)] + 7.5\log(r/d)\,, \tag{11}$$

The SEL at the test distance d, i.e. SEL(d), in Eq. 11, is a function of $L_{A,mx}(d)$, as described in Section III C. Therefore, according to Eq. 11, knowledge of $L_{A,mx}$ leads directly into obtaining the SEL NPD curves. Hence, the key objective of the framework is estimating variations $\Delta L_{A,mx}$.

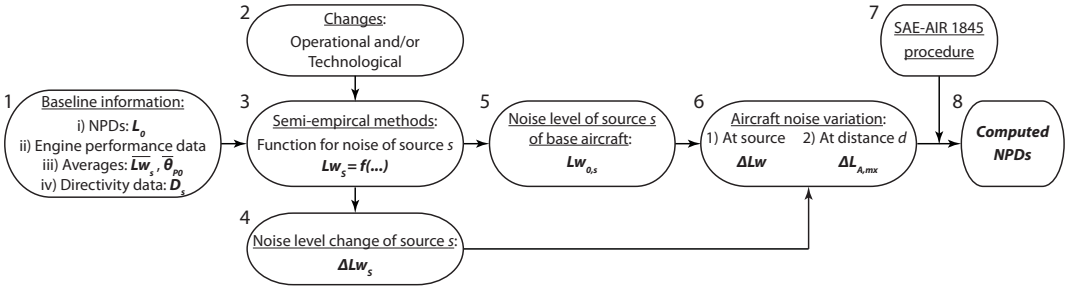

Fig. 4 The framework flowchart.

B. Aircraft noise variation due to changes

Aircraft noise level variation $\Delta L_{A,mx}$ due to technological and/or operational changes is obtained with Eq. 8. The processes of acquiring each parameter of that equation are described next with reference to the flowchart in Fig. 4, where elements are numbered for reference.

Starting from the baseline information (flowchart element 1):

- Angle θ_{P0} is either given or assigned the average value provided by NASA [14].
- Baseline aircraft directivity D_0 is calculated with Eq. 4. In case of lack of accurate directivities D_s describing each source s, these can be approximated with average values, like the ones included in ANOPP [13].

The level change ΔLw in Eq. 8 can be expressed as

$$\Delta Lw = 10 \log \left(\sum_{s=1}^{N} 10^{\frac{Lw_{0,s} + \Delta Lw_s}{10}} \right) - Lw_0 \,, \tag{12}$$

where the baseline aircraft PWL, Lw_0 is obtained from the published NPD data (e.g. from the ANP Database [8]). Whereas the noise level variations ΔLw_s of each source are estimated through the vertical procedure 2-3-4 in the flowchart that is represented by Eq. 7.

It is apparent that both equations 4 and 12 require knowledge of the sound power levels (PWL) $Lw_{0,s}$ of each individual source of the baseline aircraft. These are approximated using the procedure described in Appendix A.

Having approximated levels $Lw_{0,s}$ (element 5), the total aircraft level change ΔLw can be calculated with Eq. 12. These can be substituted in Eq. 8 to give $\Delta L_{A,mx}(d, j)$ (element 6.2) for slant distance d and engine power settings j. This yields the sought $L_{A,mx}$ values, that can be

generalised into other distances using the SAE AIR1845 procedure [9] to get the $L_{A,mx}$ NPDs. SEL NPDs can then be acquired from the procedure described in the following section.

C. Estimation of SEL at test distance

With reference to the test flyover of Fig. 2, the SEL at slant distance d is [5]:

$$\mathrm{SEL} = 10\log\left(\int_{t_1}^{t_2} 10^{\frac{\mathrm{SPL}}{10}}\,\mathrm{d}t\right), \tag{13}$$

where the interval $[t_1, t_2]$ correspond to the flyover period for which the instantaneous SPL

$$\mathrm{SPL}(t) = Lw + 10\log\left[\frac{D(t)}{R(t)^2}\right] + C\,, \tag{14}$$

is within 10 dB of $L_{A,mx}$. Considering an airspeed of 160 knots and a time increment of 0.5 seconds, as recommended by the SAE AIR1845 procedure [9], distances $R(t)$ corresponding to each time increment of the test flyover can be calculated. Whereas Equation 12 suggests that the aircraft PWL is

$$Lw = Lw_0 + \Delta Lw\,. \tag{15}$$

These parameters are inserted in Eq. 14 to yield the SPLs required to calculate SEL(d) with Eq. 13. SEL(d) is substituted in Eq. 11 to give the SEL(r) and develop the SEL NPDs.

IV. Demonstrations of the Framework

A. Inputs and assumptions

Having described the framework architecture in complete generality, its functionality is next demonstrated in more detail using specific noise prediction methods, datasets and assumptions. These are listed below:

- The noise prediction methods employed are the semi-empirical ones of Heidmann's [19] for fan noise, Fink [21] for airframe noise and the Lighthill's acoustic analogy [20] for jet noise.
- The experimental dataset provided by NASA [14] that includes:

  - Average noise levels of individual noise sources among aircraft of similar sizes (aircraft-size categories) at takeoff and landing certification conditions, and
  - Average polar angles of $L_{A,mx}$ occurrence for each aircraft-size category and operation (takeoff, landing). The aircraft-size categories defined in reference [14] are Business jet, Small twin, Medium twin and Large quad.

- Noise and performance information from the ANP database [8].
- Directivity data in NASA's ANOPP [13].
- The aircraft noise sources considered are only the significant ones. For turbofan-powered aircraft, it is generally acknowledged that these are the jet, the fan and the airframe [14]. This reduces the number of noise prediction models employed by the framework and hence the inputs required, without producing significant error.
- If the impact of new noise reduction technologies (e.g. nacelle acoustic liners) and/or design differences is known, this can easily be incorporated in the framework. For instance, in the application case of Section IV C 2, the effect of chevrons and liners on jet and fan noise is considered with the addition of respective noise reductions. Likewise, the effect of a geared fan on the fan noise can be expressed by appropriately adapting the low pressure rotor speed N1 in Heidmann's method [19]. If the noise impact of new designs and/or technologies is unavailable, the effect can be approximated or assumed (e.g. based on historical trends or data available for similar sources).

B. Formation of noise variation equations for each noise source

First we implement Eq. 7 to obtain flowchart element 4; i.e. the noise variation for each individual aircraft noise source (fan, jet, airframe) due to changes based on the semi-empirical methods chosen earlier. To incorporate the effect of changing engine power settings, the derived equations are modified to include the parameter of gross thrust F_G. For reference, Fig. 5 shows a sketch of a turbofan engine.

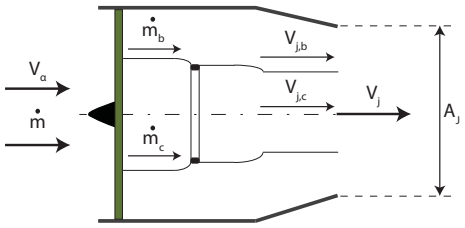

Fig. 5 Schematic representation of a turbofan engine.

1. *Jet Noise*

Lighthill's acoustic analogy [20] implies that the jet acoustic power satisfies

$$W_j \propto \rho_j A_j V_j^8 \,. \tag{16}$$

Introducing F_G and an effective velocity, such as the one suggested by Michel [23] to account for the flight speed effects, Eq. 16 becomes

$$W_j \propto F_G V_e^6 \,, \tag{17}$$

with $V_e = f(V_j, V_{ac})$. Thus, the jet PWL change due to a change of gross thrust is expressed as

$$\Delta Lw_j = 10 \log \frac{F_G'}{F_G} + 60 \log \frac{V_e'}{V_e} \,, \tag{18}$$

where the values corresponding to the condition after the thrust change are denoted with a dash.

2. *Fan Noise*

The fan is associated with both broadband and tonal noise components [18]. According to Heidmann [19], the total SPL of the fan is obtained using a logarithmic sum (analogous to Eq. 1), where the SPL of each fan noise component, κ, of a fan stage is obtained from

$$\mathrm{SPL}_\kappa = \mathrm{SPL}_{ref} - 20 \log \frac{\Delta T}{\Delta T_{ref}} - 10 \log \frac{\dot{m}}{\dot{m}_{ref}} - f_\kappa \,. \tag{19}$$

Function f_κ describes spectral and directivity properties of fan noise component, κ and the relationship between the operating tip Mach number M_T (i.e. throttle setting) and the noise generated. The total temperature rise across the fan stage with isentropic efficiency η_c is given by [24]

$$\Delta T = \frac{V_{j,b}^2 - V_{ac}^2}{2 c_p \eta_c} \,, \tag{20}$$

where c_p is the specific heat in constant pressure. Substituting ΔT in Eq. 19 and performing algebraic manipulations lead to the following expression for the fan PWL change

$$\Delta Lw_{f,\kappa} = 20\log\left(\frac{V_{j,b}'^2 - V_{ac}'^2}{V_{j,b}^2 - V_{ac}^2}\right) + 10\log\frac{F_G'}{F_G} - 10\log\frac{V_j'}{V_j} + \Delta f_\kappa\,. \tag{21}$$

For a fixed fan, Δf_κ essentially depends on M_T, which is a function of the publicly available fan diameter d_f and low pressure rotor speed N1.

The velocities V_j, $V_{j,b}$ required by Equations 18 and 21 are estimated using the procedure in Appendix B.

3. Airframe Noise

Fink [21] suggests that noise acoustic power for each airframe component τ is given by a function of the form

$$W_\tau = KGV_{ac}^a\,, \tag{22}$$

where a and K are constants and G is a geometry function that varies among airframe components. The PWL change of a given airframe component τ is expressed as

$$\Delta Lw_\tau = 10\log\frac{G_\tau'}{G_\tau} + 10a\log\frac{V_{ac}'}{V_{ac}}\,. \tag{23}$$

Fink [21] gives $a = 5$ for wings or tails and $a = 6$ for flaps and landing gears. It is apparent that for a fixed aircraft and landing gear state, parameters that influence airframe noise are airspeed V_{ac} and flap deflection angle δ. The flap function specified in [21] is

$$G_f = \frac{A}{b^2}\sin^2\delta, \tag{24}$$

where A and b are the flap area and flap span respectively. Since geometry parameters are fixed, the PWL change due to flap deflection angle change at a given airspeed is given by

$$\Delta Lw_{a,f} = 10\log\frac{\sin^2\delta'}{\sin^2\delta}\,. \tag{25}$$

If landing gear state is not fixed, then the noise due to landing gear deployment can be calculated similarly, using parameters a, K and G, as specified in [21].

C. Validation

We validate the model by comparing predicted and published SEL NPD curves. Two validation cases are presented below.

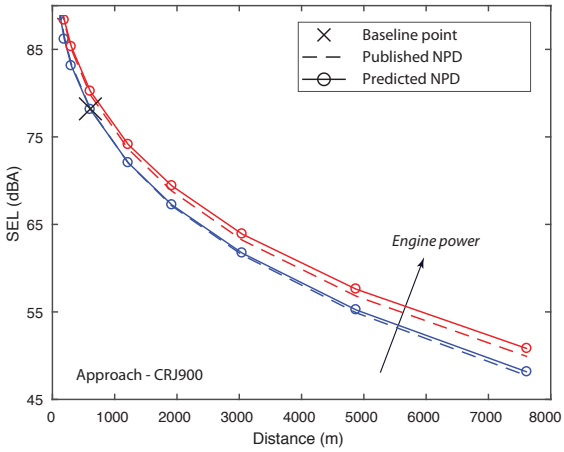

Fig. 6 Validation case: Comparison between published and estimated NPD curves for the Bombardier CRJ900 at approach configuration.

1. NPDs for the Bombardier CRJ900

The first validation case involves computing NPD curves for an existing aircraft, namely the Bombardier CRJ900 at approach, and certify that it matches the published ones. A point on the published NPD curves is chosen as baseline point. This point should lie within the standard slant distance range for flyover experimental measurements, as specified by SAE AIR 1845 [9], i.e. from 100 m to 800 m. This condition is satisfied in all examined scenarios thereafter. For the Bombardier CRJ900 example, the chosen baseline NPD point is the one corresponding to slant distance of 609 m. Figure 6 compares the published (dashed lines) with the predicted NPD curves (continuous lines). The base point is marked with a cross, whereas calculated points are marked with a circle.

2. NPDs for the B737-800 and the B747-8

The second validation case demonstrates the framework capability of estimating NPDs for newer generation aircraft, starting from the noise and performance data of their predecessors. More specifically, we derive the NPD curves for Boeing B737-800 and B747-8 using as baseline the NPD curves of their predecessors, the B737-400 and B747-400 respectively. Technological changes between older (i.e. the B737-400 and the B747-400) and newer (i.e. the B737-800 and the B747-8) models

Table 1 Input engine parameters for the Boeing 737-400 and its successor, the 737-800.

Aircraft	737-400	737-800
BPR	6	5.3
Fan diameter (m)	1.5	1.55
FPR	1.64	1.67
OPR	30.6	32.3
Max. sea level static thrust (kN)	104.5	107.6
Airflow at max thrust (kg/s)	322	342
Max. low press. rotor speed, N1 (rpm)	5490	5382

are known and listed in Tables 1 and 2. This allows estimating the aircraft noise variation due to these changes, which leads in constructing the NPDs for the newer models.

Table 2 Input engine parameters for the Boeing 747-400 and its successor, the 747-8.

Aircraft	747-400	747-8
BPR	5.1	8.6
Fan diameter (m)	2.36	2.66
FPR	1.73	1.65
OPR	30.13	44.7
Max. sea level static thrust (kN)	254	302.5
Airflow at max thrust (kg/s)	800	1042
Max. low press. rotor speed, N1 (rpm)	3835	3026

Regarding the B747-8 case, additional noise level changes have been considered, originating from two technological advances; a) the chevron on the trailing edge that reduces jet noise, b) the sound-absorbing inlet liner in the nacelle that attenuates fan noise. Based on references [2, 36–38] fan and jet noise are additionally attenuated by 5 dB and 3 dB respectively, in order to account for these technological improvements. Figure 7 compares the published and predicted takeoff NPD curves, using the same notation as previously.

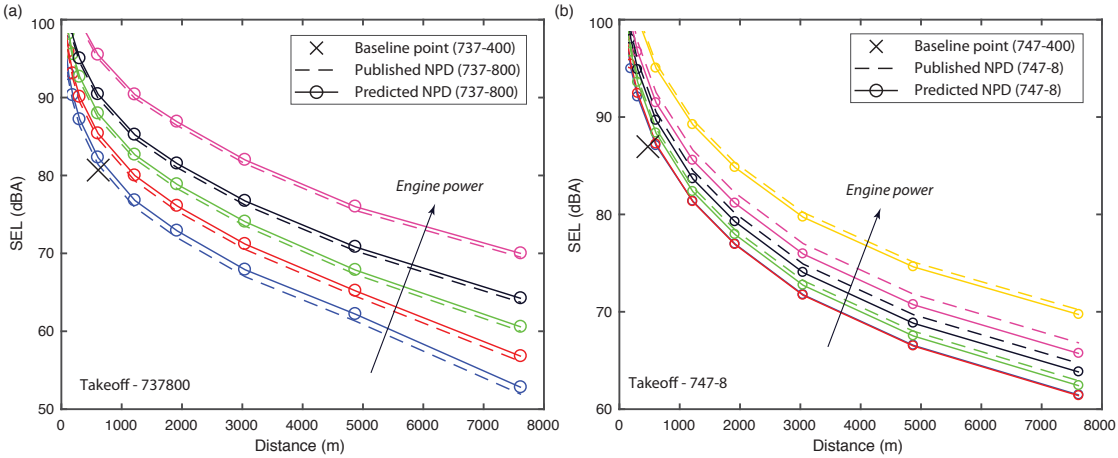

Fig. 7 Validation cases: Comparison between published and predicted NPD curves for two recent aircraft models derived based on noise and design data of their predecessors. (a) 737-800 based on the 737-400, (b) 747-8 based on the 747-400.

D. Applications

The two examples presented in this section are representative of contemporary scenarios. The first one features aircraft configuration changes due to operational alteration. The second one involves technological changes and features a future aircraft concept, the blended wing body (BWB) aircraft. All results including the validation in the previous paragraph are discussed altogether in the next section.

1. NPDs for steeper approach operation

NPD curves are derived for an Airbus A320 at a steeper approach configuration. Steeper approach is a noise abatement landing procedure already implemented in some airports (e.g. London City airport) that includes a glide slope of 5.5° (the standard slope is 3°). This procedure imposes aircraft performance restrictions that limits the types of aircraft which can use the airport. Based on flyability tests in references [15] and [16], we assume that an Airbus A320 can perform a 5.5° descent, if the flaps are fully extracted. Figure 8 shows the NPD curves for the steeper descent configuration (i.e. the noise levels when flaps are fully extended) versus the NPD curves at standard approach configuration. A steep descent configuration increases the aircraft PWL due to augmenting the

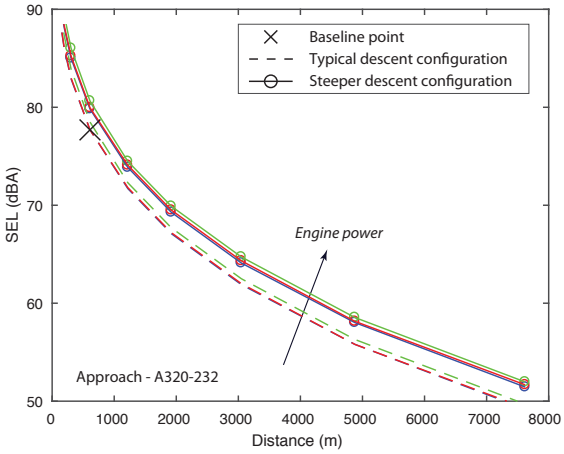

Fig. 8 Application case, operational change: Predicted NPD curves for the A320-232 at steeper descent configuration (solid lines). NPDs for the conventional configuration are shown with dashed lines for comparison.

flap deflection angle (as implied by Eq. 25). Still, steep approach is considered a noise abatement procedure because that PWL increase is offset by the noise benefits from increasing approach slope and hence the distance between aircraft path and the ground, as shown in e.g. reference [15]. Also, it must be noted that a steeper approach is associated with increased drag and therefore it is likely to be accompanied by an increase in engine power requirement. This increase can be evaluated through aircraft performance tools so that the curve assigned to the correct engine power setting is read when using the derived NPD curves.

2. NPDs for a blended wing body (BWB) aircraft

Blended wing body (BWB) aircraft are envisioned to have their engines mounted on top of the airframe, shielding a significant portion of engine noise [2]. It is assumed that the airframe shields engine noise radiated at polar angles ranging from 45° to 135°. Hence, the engine noise sources directivity can be roughly represented by the graph in Fig. 9 (a), where the directivity factor within the shielding range is set to zero for all engine sources. Substituting these directivities in Eq. 4 produces a similarly-shaped lumped aircraft directivity, plotted in Fig. 9 (b). It is seen that the shielding effect is prominent at takeoff, when engine noise dominates. Equation 4 suggests that the

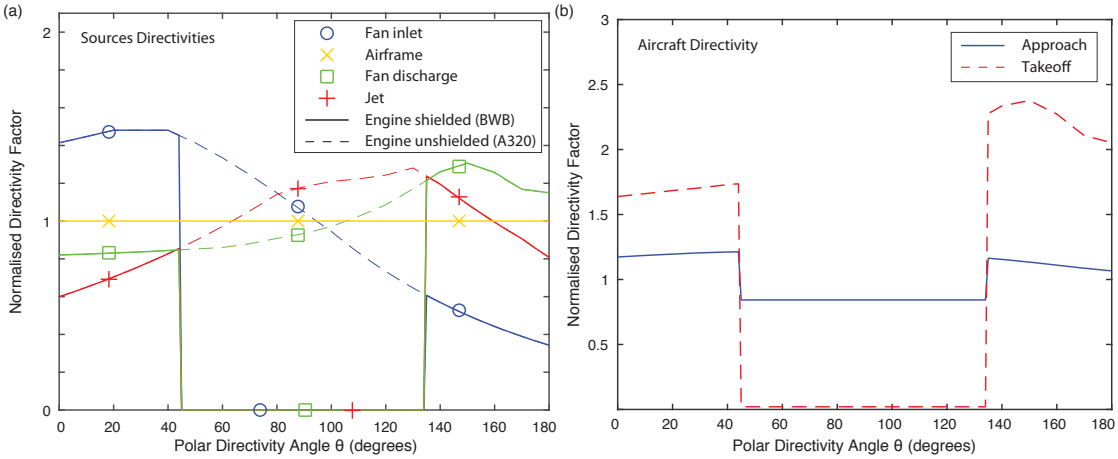

Fig. 9 (a) Source directivities for the test BWB, (b) Lumped directivity for the whole aircraft at takeoff and approach, at the corresponding standard NPD engine power settings (obtained from the ANP Database [8]).

aircraft lumped directivity depends on each source sound level $Lw_s(j)$, which in turn is a function of engine power setting. For the comparison to be clearer, Fig. 9 (b) only shows the lumped directivities for the BWB at the standard A320-232 engine power settings. The recommended procedure for calculating these standard power settings is thoroughly described in references [5, 9].

The methodology presented in Section III and more specifically Eq. 8 includes sources directivities, which implies that the framework can generate NPDs for scenarios involving directivity variations. For demonstrating this capability, the base aircraft is taken to be an A320-232; so, the test BWB is assumed to have identical thrust requirements as the A320-232 and therefore is equipped with the engines of the A320-232. Figure 10 compares the takeoff and approach SEL NPD curves of the A320-232 with the ones generated for the test BWB. As said above, both aircraft have identical engines and thrust requirements and therefore, the noise exposure reduction is due to the engine noise shielding, i.e. the directivity change. As expected, the shielding effect is more apparent in the takeoff case, when engine noise dominates. The dotted lines in the approach plot of Fig. 10 represent NPDs for the BWB including a 4 dB airframe noise reduction due to projected noise reduction technologies for airframe noise sources described in [28]. The influence of the fuselage shape difference between the BWB and A320 is discussed in Section V.

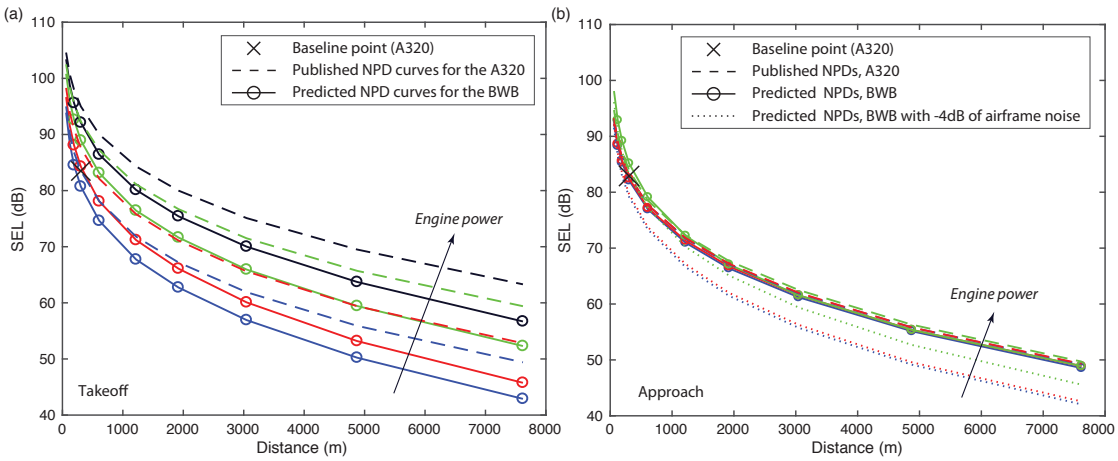

Fig. 10 Application case, technological change: Generated NPD curves for a BWB aircraft at (a) Takeoff, and (b) Approach. The A320-232 NPD curves are shown with dashed lines for comparison.

The effect of engine noise shielding on ground noise contours was assessed by computing (in INM [6]) the 85-SEL noise contour of the BWB aircraft and the A320-232 aircraft using the NPD curves shown in Fig. 10. An overall reduction of 65% in 85-SEL contour at take-off condition was found between the BWB and A320-232 aircraft, as illustrated in Fig. 11. This result is consistent with Thomas and Guo [29], who found a near identical 65.7% reduction in ground noise contour of a BWB as compared to a 2025 technology tube-and-wing aircraft with engines installed under the wing.

V. Discussion

This Section gives a critical review of both the benefits and limitations of the framework developed. To demonstrate the framework's validity, the NPD curves derived for existing aircraft were compared with the published ones. This process showed an excellent agreement, obtaining an average error of about ±1.5 dB, which is within the tolerance suggested in ECAC Doc 29 [5] and in similar noise prediction studies like these in references [1, 33]. The fact that the ANOPP directivity data were used in all cases did not produce significant error in terms of NPD curves estimation. Overall, the general agreement supports the validity of the framework and the trustworthiness of the NPD curves derived for contemporary scenarios.

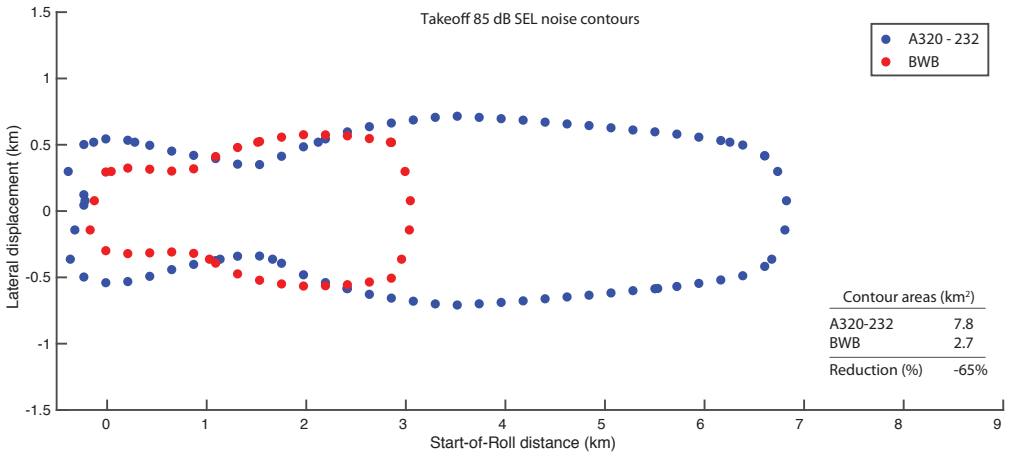

Fig. 11 85-SEL noise exposure contours of the BWB aircraft and the A320-232 aircraft as derived using the NPD curves of Fig. 10.

In the steeper descent study, it was assumed for simplicity that landing gears deployment occurs at a fixed horizontal distance from the airport, which is independent of approach angle. So that the only configuration difference between conventional and steeper descent is the flap deflection angle. As expected, this configuration change results into raising the aircraft SEL by about 1–1.5 dB. If the landing gears are extracted at different lateral distances from the airport, a new configuration change between standard and steeper descent arises. This introduces an additional level change ΔLw_a into the model that can be obtained through Fink's method for airframe noise. Taking into account that landing gear is one of the most significant sources of airframe noise, such a configuration change is likely to alter the overall approach noise exposure level and hence should not be ignored.

Looking at the BWB example, the expected noise reduction trend with this technology is estimated using the developed framework. A notable decrease of takeoff SEL NPDs (around 5 dB) was observed due to the engine noise shielding. In approach configuration, when airframe noise dominates over engine noise [12], the benefits of shielding were degraded and the decrease of SEL NPDs was only noticeable at the highest engine power setting. Since the purpose of this example was to demonstrate the applicability of the developed framework to new aircraft designs, the shielding was simply represented by setting the directivity factor to zero at polar angles ranging from 45° to 135°. This range was chosen arbitrarily. Actual shielding range will be affected by diffraction effects but

more importantly will be determined by the engine design and its position on the fuselage, as well as on the fuselage dimensions. Such design characteristics are likely to be publicly available, as are currently for the existing aircraft. Furthermore BWB prototypes suggest that their fuselage shape will deviate from the traditional tube and wing shape and therefore airframe noise contribution will differ from that of the A320, which was the baseline aircraft in this example. BWB are conceived to have a clean, lifting body airframe with no high-lift devices [2], which could result in airframe noise reductions of 12 dB [35]. This reduction could have been accounted for in the present example but this was beyond demonstrating the framework capabilities. Moreover, BWB aircraft are expected to achieve low approach velocities and steeper glide slopes that will further reduce the airframe noise (which, according to Fink [21] scales with the 5th power of airspeed) and consequently the overall aircraft noise at approach operations.

Overall, the examples presented above highlighted two additional characteristics of the framework. Firstly, its usefulness even in the absence of a baseline scenario. This is because noise impact (and parametric) studies can still be implemented by comparing different configurations to an hypothetical base scenario. In essence, this is what was done in the BWB example, where the baseline aircraft was conveniently taken to be the A320-232, despite the aforementioned fuselage shape differences. Still, this did not impede the extraction of useful outcomes as to the potential noise benefits of the BWB. Secondly, since the framework essentially replaces the experimental part of the standard SAE AIR1845 methodology, it also bypasses errors associated with such field measurements, due to: a) pilots failing to accurately maintain the nominal flight profile, engine power setting and configuration, b) inaccuracies in recording the test aircraft position and synchronising it with noise measurements, and c) varying atmospheric conditions during testing. Nevertheless, the proposed framework is also associated with uncertainty arising from a number of reasons further discussed below.

Uncertainties and errors embodied in the baseline scenario noise levels are independent of the effectiveness and validity of the framework, for two reasons: a) baseline error only affects the base point and does not scale within the framework, and more importantly b) the proposed framework does not intend to predict absolute noise values, rather, it has a comparative nature where only

changes in noise level are estimated and hence baseline scenario errors do not prevent its ability to correctly render trends.

Error introduced from simplifications and from using average data was demonstrated in Section IV C of this paper to be acceptable. Also, it is well compensated by the substantial advantage of requiring just a few publicly available inputs. Using average values offers the following benefits: a) aircraft of similar noise and performance characteristics are represented by only one base aircraft, b) dependence on specific aircraft details is bypassed, c) average noise levels for individual aircraft noise sources (fan, jet, etc) that are publicly available can be used (in contrast, such data are normally proprietary to manufacturers for specific aircraft), d) this approach is very useful and completely valid in the study of future aircraft designs, where only the specifications of a generic (or representative) aircraft of a specific category are considered, and e) the overall complexity of the method is reduced. Complexity is further reduced by only including the dominant aircraft noise sources. Consequently, the framework has low computational requirements and produces NPDs for a given scenario within seconds.

There is of course a mathematical error associated with the way the framework estimates changes in noise sources. However, the examples presented in this paper demonstrated that if appropriate noise prediction methods for individual aircraft noise sources are used, then the error is likely to be small. More importantly, it was pointed out earlier that noise prediction methods for individual noise sources are indispensable for the framework functionality. As aircraft and propulsion system design evolves, these methods tend to become inaccurate and even obsolete. For example, Fink's method may be unsuitable for modelling the noise characteristics of advanced high-lift devices, such as the Krueger flap. Furthermore, future aircraft designs may be associated with different and/or new significant noise sources. Although the accuracy of the framework presented in this paper depends on the level of adaptation of noise prediction methods to new technologies and/or the development of new ones, it is independent of specific methods (e.g. Fink's for airframe noise). New methods for (existing or new) individual aircraft noise sources (e.g. higher fidelity methods incorporated into NASA's next generation aircraft noise prediction program, ANOPP2 [25], such as the recently developed Boeing methods for Kruger flap [26] and landing gear [27]) can be introduced

within the framework in order to achieve a better estimation of NPDs. Also, installation effects due to different configurations (e.g different engine positioning) can be accounted for by either using appropriate higher fidelity methods, or applying empirically-based corrections (e.g. in the earlier-presented BWB example, corrections were directly applied on noise radiated within the shielding range).

The estimation of engine stream velocities (Appendix B) is based on a number of assumptions according to references [30–32]. These assumptions are: a) the gas properties are fixed across the components, b) the flow is one-dimensional c) the power needed to drive the fan and high-pressure (HP) compressor equals the power delivered by the low pressure (LP) and HP turbine respectively, and d) the rotating machinery components are assigned fixed, empirically derived polytropic efficiencies that represent a technology level rather than a certain engine. According to [30–32], assumptions a) to c) produce insignificant stream velocities error. Regarding the last mentioned assumption, the average variation of jet velocities (that are the parameters sought from the cycle analysis) resulting from altering efficiencies by 10% was found to be less than 3%. This produces an average noise level error in the order of 0.1 dB. Overall, it is judged that the thermodynamic engine cycle analysis performed delivers sufficiently accurate inputs to the framework.

Since the framework uses the computational part of the standard SAE AIR1845 procedure for developing NPD data, uncertainties associated with this standard are briefly listed below:

- For most existing aircraft the publicly accessible spectra are average spectral shapes for aircraft with resembling spectral characteristics, representative for just the time of $L_{A,mx}$ occurrence. Even in the ideal case when spectra data is available for the full time history of the test flyover, some discrepancies have been reported between NPD data and field measurements, especially in the larger distances and at frequencies above 4 kHz [17, 18]. This suggests that NPD data are likely to incorporate discrepancies that may be severe for some aircraft types, particularly at larger distances.

- The procedure assumes that the polar angle when $L_{A,mx}$ occurs is independent from distance, which means that the effect of atmospheric absorption at large distances on that polar angle is neglected. Although an empirical factor is used to correct that, uncertainty still remains

due to the fact that the same factor is used for all aircraft and distances.

The only source of uncertainty that is generated exclusively within the framework is the procedure to estimate the individual noise source levels for the baseline aircraft. As described in Section A, this essentially involves fitting of predicted NPD curves to published ones. This implies that NPD uncertainties described in the previous paragraph influence the resulting noise source levels. Furthermore, the fact that noise source levels for all aircraft within a given size category are derived through small variations of the same relative noise levels implies the assumption that all aircraft (within that category) have the same dominant noise sources. Although this is a reasonable assumption, since parameters affecting noise (e.g. maximum sea level static thrust, BPR, fan diameter) are generally similar for turbofan engines applicable to each aircraft size-category, some exceptions could exist. To minimise the error arising from this assumption, baseline aircraft used in the above examples are among the ones representing the NASA size-classes defined in reference [14] (i.e. the A320, B737-400, B747-400).

VI. Conclusion

This paper presents a new framework for generating NPD data, that only uses publicly available inputs and bypasses the need for costly, tedious and sometimes confidential experimental measurements. Using the developed framework, NPDs for future aircraft designs can be obtained, which allow the investigation of the potential benefit of such designs for reducing the impact of aviation noise around airports. Moreover, the developed framework might be used to explore different technology options, and thus, proposing the technology platforms more likely to achieve the lowest noise impact on residents around airports.

The framework combines noise prediction methods for individual sources with aircraft noise and performance data to estimate noise variation with respect to a baseline scenario, where noise levels are known. The framework can incorporate any potential new prediction methods for existing or new noise sources. Computational requirements are low and results are promptly obtained; generating NPD data for a given scenario is a matter of few seconds. Validation of the framework was achieved by calculating NPD curves for existing scenarios and comparing them to the published

ones. Whereas its applicability was demonstrated through developing NPD curves for scenarios involving advanced technological and operational concepts, such as the BWB aircraft and the steeper approach. Results obtained are sufficiently accurate and exhibit the expected trends. Even in the absence of a baseline scenario, the framework showed promising capabilities in capturing the correct trends. As indicated above, this could be extremely useful in conducting parametric or optimisation studies involving future aircraft.

It is therefore concluded that the framework has the potential to providing good NPDs estimates for future aircraft designs and contemporary operations in a relatively quick time frame. Clearly, its ability to operate based only on non-confidential inputs and some average data, as well as using only the significant noise sources, are significant advantages. While average public data suffice to produce satisfactory results, aircraft-specific data can be easily incorporated into the framework, if available, to increase accuracy. Errors associated with the thermodynamic cycle analysis are not significant, whereas uncertainties linked to the standard SAE AIR 1845 NPD development methodology could influence results at larger distances but without considerably affecting the overall trends.

Further work includes exploring the possibility of introducing new processes for calculating NPD points, in an effort to reduce the dependance on the standard SAE AIR1845 procedure and avoid the associated uncertainties. Currently, the framework is being used to investigate the optimum, in terms of noise, takeoff and approach angles of existing civil aircraft. Additionally, the framework is being employed to predict the noise trends of future aircraft concepts, such as the Turboelectric DP (TeDP)[39] and Universally-Electric [40] aircraft that consist of a power unit (turboshaft and batteries respectively) that drives electrically, rather than mechanically, a number of electric propulsors. Electric propulsors incorporate a fan and jet and therefore the framework described in this paper is used with existing fan and jet noise prediction methods to realise preliminary noise estimations. Also, these future aircraft concepts are envisaged to use distributed propulsion (DP), i.e. disperse thrust among multiple propulsors; DP is anticipated as one of the most suitable and efficient options for powering future aircraft [39]. So another aspect of the future aircraft study is to determine the optimum number of propulsors on DP systems, in terms of noise.

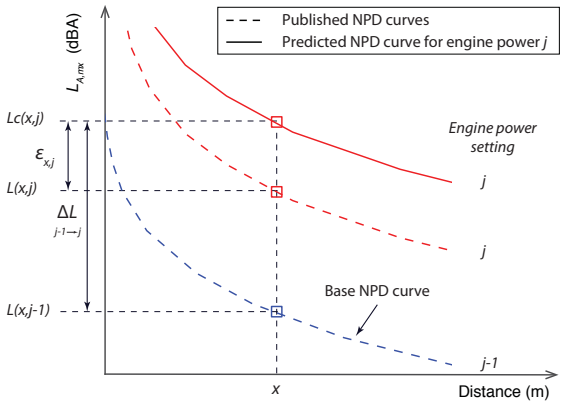

Fig. 12 Graphical interpretation of the procedure to estimate individual noise source levels $Lw0,s$ of the baseline aircraft. Initially, $Lw0,s$ are assigned the values of the NASA average levels $\overline{Lw_s}$. This produces an error ε between the predicted and published NPD curves. The aim is to slightly vary values $\overline{Lw_s}$ until the error ε becomes minimum for every distance x. This yields the estimated levels $Lw0,s$.

Appendix A: Estimating levels of individual noise sources of the baseline aircraft

$Lw_{0,s}$ of each individual source of the baseline aircraft are normally proprietary to manufacturers. Hence, we approximate them through a procedure that exploits three publicly available components: a) NPD data for the baseline aircraft, e.g. from the ANP database, b) average noise levels of individual noise sources, e.g. the dataset found in [14], and c) semi-empirical noise prediction methods for each source. The technique is represented by the horizontal procedure 1-3-5 of the flowchart in Fig. 4.

The general idea involves reproducing NPDs for baseline scenarios and fitting them to the published ones. The variables in this fitting process are the sought baseline noise source levels $Lw_{0,s}$ that are initially assigned the values of the average levels $\overline{Lw_s}$ provided by NASA [14]. $\overline{Lw_s}$ are fine-tuned until the error $\varepsilon_{d,j}$ between predicted and published NPD curves becomes minimum. The procedure is described below in detail with reference to Fig. 12.

To begin with, the sought baseline noise source levels (flowchart element 5) are written as the sum of the averages and a correction α_s, respective to each source s:

$$Lw_{0,s} = \overline{Lw_s} + \alpha_s \tag{A1}$$

To avoid unrealistic results, two conditions are required; a) corrections α_s are restricted to within 3 dB, and b) the logarithmic sum of $Lw_{0,s}$ should equal the noise level Lw_0 of the whole baseline aircraft.

Next, we chose a point on the baseline $L_{A,mx}$ NPD curve, corresponding to engine power setting $j-1$, distance x and maximum level $L(x, j-1)$. We back-propagate (with Eq. 2) this level to the aircraft, in order to get the aircraft PWL, Lw_0. Back-propagation makes use of the angle at the time when $L_{A,mx}$ occurs; as said previously, this is either known or approximated with published averages. We then estimate the level variation ΔLw_s of each noise source due to the engine power setting change from $j-1$ to j, using Eq. 7 (i.e. the vertical procedure 2-3-4 in the flowchart).

Variation ΔLw_s is then substituted into Eq. 12 along with levels in Eq. A1 to obtain the whole aircraft PWL variation ΔLw (flowchart element 6.1). Aircraft lumped directivity D is updated with Eq. 4 to reflect the corrected (with Eq. A1) $Lw_{0,s}$. Variation $\Delta L(x, j)$ can now be obtained from Eq. 8, yielding the calculated NPD level $Lc(x, j)$ through Eq. 9.

This procedure is repeated for different corrections α_s until the error between predicted and published NPD level

$$\varepsilon_{d,j} = |Lc(x, j) - L_0(x, j)| \tag{A2}$$

at any distance x and engine power j is minimised. The resulting levels $Lw_{0,s}$ are accepted as the individual source levels for the baseline aircraft.

Appendix B: Estimation of inputs to the noise variation equations for individual sources

One way of estimating the mixed and bypass jet velocities (V_j, $V_{j,b}$) is to treat the turbofan dual stream engine as an equivalent single stream that generates identical amount of thrust F. This equivalent single stream engine can be associated with an equivalent (often termed 'mixed') jet velocity V_j and jet temperature T_j.

The rated jet mixed velocity of the baseline turbofan engine is directly obtained through the definition of static thrust [24], with

$$V_{j,\infty} = \frac{F_\infty}{\dot{m}_\infty}\,, \tag{B1}$$

where the maximum sea level static thrust F_∞ and the associated engine airflow $\dot{m}_\infty$ are freely available quantities.

Then, ignoring any effective area effects, the geometric jet area is evaluated based on the definition of mass flow [24] with

$$A_j = \frac{\dot{m}_\infty}{\rho_{j,\infty} V_{j,\infty}}\,, \tag{B2}$$

where the fully expanded jet density $\rho_{j,\infty}$ can be acquired from

$$\rho_{j,\infty} = \frac{P_a}{R_s T_{tj,\infty}}\,, \tag{B3}$$

where R_s is the specific gas constant of air and P_a denotes the atmospheric pressure. The total mixed jet temperature $T_{tj,\infty}$ of the equivalent single stream engine at rated thrust is obtained from a turbofan engine cycle thermodynamic analysis [30–32]. This is done under the assumption that the core stream jet temperature at rated thrust is equal to the operational limit of the low pressure turbine (LPT) exit temperature, which is publicly available in the EASA TCDS certificates [34].

Having calculated A_j, then for a fixed net thrust F_N and airspeed, the mixed jet velocity is the positive root of the polynomial

$$V_j^2 - V_{ac} V_j - \frac{F_N}{\rho_j A_j} = 0\,, \tag{B4}$$

that derives from the net thrust definition. An expression for the bypass stream jet velocity, which is the remaining parameter required for assessing the fan level change in Eq. 21, is directly worked out starting from the fact that the total engine thrust is the sum of that generated by each stream. With μ being the turbofan bypass ratio, the final expression is:

$$V_{j,b} = \frac{V_j(1+\mu) - V_c}{\mu}\,. \tag{B5}$$

In the equations above, the jet density ρ_j and the core velocity V_c are approximated from the engine cycle thermodynamic analysis.

Appendix C: Brief review of the SAE AIR1845 procedure

This Appendix lists the main steps of the SAE AIR 1845 [9] procedure for developing NPD relationships.

- Atmospheric conditions for each sound recording are established experimentally.
- The terrain around the microphones is flat and unobstructed.
- The test flight path is parallel to the ground (SAE AIR 1845 describes it as 'nominally level') at a nominal height ranging from 100 m to 800 m.

- Noise measurements are made directly under the flight path so are unaffected by lateral attenuation.
- The aircraft configuration remains constant throughout each flyover duration.
- Flyover effective duration is normally determined by the 10 dB down-time (i.e. the period during which the noise level is within 10 dB of the maximum level).
- The noise is recorded at 0.5 seconds intervals. SPLs are obtained for the 24 1/3-octave-bands with centre frequencies from 50 to 10000Hz.
- Measured SPLs are corrected for instrument calibration and adjusted to account for differences between actual and reference atmospheric conditions.
- A flyover at the nominal height is repeated for each engine power setting.
- The noise at the remaining NPD standard distances is then evaluated using extrapolation, accounting for effects of spherical wave spreading, atmospheric absorption as well as for differences on the effective duration.

Acknowledgments

A. J. Torija acknowledges the funding provided by the Engineering and Physical Science research Council (Grant No. EP/M026868/1).

References

[1] Bernardo, J. E., Kirby, M., and Mavris, D., "Development of a Rapid Fleet-Level Noise Computation Model," *Journal of Aircraft*, Vol. 52, No. 3, 2015, pp. 721–733, doi:10.2514/1.C032503.

[2] Rizzi, S. A., Aumann, A. R., Lopes, L. V., and Burley, C. L., "Auralization of Hybrid Wing-Body Aircraft Flyover Noise from System Noise Predictions," *Journal of Aircraft*, Vol. 51, No. 6, 2014, pp. 1914–1926, doi:10.2514/1.C032572.

[3] International Civil Aircraft Organization (ICAO), "Environmental Protection, Vol. 1, Aircraft noise," Annex 16, Montreal, 2008.

[4] UK Department for Transport, "Noise Exposure Contours Around London Airports," URL: https://www.gov.uk/government/publications/noise-exposure-contours-around-london-airports [retrieved: March 2017].

[5] "ECAC.CEAC Doc 29, 4th ed., Report on Standard Method of Computing Noise Contours around Civil Airports," European Civil Aviation Conference, Document 29, Paris, URL: https://www.ecac-ceac.org/ecac-docs [retrieved March 2017].

[6] Boeker, E. R., Dinges, E., He, B., Fleming, G., Roof, J. C., Gerbi, J. P., Rapoza, S. A., and Hemann, J., "Integrated Noise Model (INM) Version 7.0 Technical Manual," Federal Aviation Administration (FAA) Rept. FAA-AEE-08-01, Washington, D.C., 2008.

[7] Federal Aviation Administration, "Aviation Environmental Design Tool (AEDT) Version 2c," URL: https://aedt.faa.gov/2c_information.aspx [retrieved: March 2017].

[8] Eurocontrol Experimental Centre, "Aircraft Noise and Performance (ANP) Database v2.1," [online database], URL: http://www.aircraftnoisemodel.org [cited March 2017].

[9] SAE International, "Procedure for the Calculation of Aircraft Noise in the Vicinity of Airports," SAE AIR1845A, 2012.

[10] Ollerhead, J. B., Rhodes, D. P., Viinikainen, M. S., Monkman, D. J., and Woodley, A. C., "The UK Civil Aircraft Noise Contour Model ANCON: Improvements in Version 2," Environmental Research and Consultancy Dept., U.K. Civil Aviation Authority, Rept. 9842, London, 1999.

[11] Torija, A. J., Self, R. H., and Flindell, I. H., "A Model for the Rapid Assessment of the Impact of Aviation Noise Near Airports," *The Journal of the Acoustical Society of America*, Vol. 141, No. 2, 2017, pp. 981–995, doi:/10.1121/1.4976053.

[12] NASA Facts, "Making Future Commercial Aircraft Quieter," NASA FS-1999-07-003-GRC, 1999.

[13] Zorumski, W. E., "Aircraft Noise Prediction Program Theoretical Manual," NASA TM-83199, Parts 1 and 2, 1982.

[14] Kumasaka, H. A., Martinez, M. M., and Weir, D. S., "Definition of 1992 Technology Aircraft Noise Levels and the Methodology for Assessing Airplane Noise Impact of Component Noise Reduction Concepts," NASA-CR-198298, 1996.

[15] Toebben, H. H., Mollwitz, V., Bertsch, L., Geister, R. M., Korn, B., and Kügler, D., "Flight Testing of Noise Abating Required Navigation Performance Procedures and Steep Approaches," *Journal of Aerospace Engineering*, Vol. 228, No. 9, 2013, pp. 1586–1597, doi:10.1177/0954410013497462.

[16] Mollwitz V., and Korn B., "Steep Segmented Approaches for Active Noise Abatement - A flyability study," *Proceedings of the 2014 Integrated Communications Navigation and Surveillance (ICNS) Con-*

ference, Herndon, 8-10 April 2014, pp. X2-1–X2-8, doi:10.1109/ICNSurv.2014.6820028.

[17] Cooper, S., and Maung, J., "Problems with the INM: Part 2 - Atmospheric attenuation," *Proceedings of the 1st Australasian Acoustical Societies' Conference*, Christchurch, New Zealand, 20-22 November 2006, pp. 99–104.

[18] Zaporozhets, O., Tokarev, V., and Attenborough, K., *Aircraft Noise: Assessment, Prediction and Control*, Spon Press, New York, 2011.

[19] Heidmann, M. F., "Interim Prediction Method for Fan and Compressor Source Noise," NASA-TM-X-71763, 1979.

[20] Lighthill, M. J., "On Sound Generated Aerodynamically. I. General Theory," *Proceedings of the Royal Society of London A: Mathematical, Physical and Engineering Sciences*, Vol. 211, No. 1107, 1952, 564–587, doi:10.1098/rspa.1952.0060.

[21] Fink, M. R., "Airframe Noise Prediction Method," Federal Aviation Administration, Rept. FAA-RD-77-29, 1977.

[22] Stone, R. J., Krejsa A. E., Clark, J. B., and Berton, J. J., "Jet Noise Modeling for Suppressed and Unsuppressed Aircraft in Simulated Flight," NASA-TM-215524, 2009.

[23] Michel, U., "Correlation of Aircraft Certification Noise Levels EPNL with Controlling Physical Parameters," *19th AIAA/CEAS Aeroacoustics Conference*, 2013, doi:10.2514/6.2013-2014.

[24] Cumpsty, N. A., *Jet Propulsion: A Simple Guide to the Aerodynamics and Thermodynamic Design and Performance of Jet Engines*, 2nd ed., Cambridge University Press, Cambridge, 2003.

[25] Lopes, L. V., and Burley, C. L., "ANOPP2 User's Manual: Version 1.2," NASA TM-2016-219342, 2016.

[26] Guo, Y., Burley, C. L., and Thomas, R. H., "Modeling and Prediction of Krueger Device Noise," *22nd AIAA/CEAS Aeroacoustics Conference*, AIAA Paper 2016-2957, 2016, doi:10.2514/6.2016-2957.

[27] Guo, Y., "A Study on Local Flow Variations for Landing Gear Noise Research," *14th AIAA/CEAS Aeroacoustics Conference (29th AIAA Aeroacoustics Conference)*, AIAA Paper 2008-2915, 2008, doi:10.2514/6.2008-2915.

[28] Guo, Y., Burley, C. L., and Thomas, R. H., "On Noise Assessment for Blended Wing Body Aircraft," *52nd Aerospace Sciences Meeting, National Harbor, Maryland*, AIAA Paper 2014-0365, 2014, doi:10.2514/6.2014-0365.

[29] Thomas, R. H., and Guo, Y., "Ground Noise Contour Prediction for a NASA Hybrid Wing Body Subsonic Transport Aircraft," *23rd AIAA/CEAS Aeroacoustics Conference*, AIAA Paper 2017-3194, 2017, doi:10.2514/6.2017-3194.

[30] Mattingly, J.D., Heiser, W. H., and Pratt, D. T., *Aircraft Engine Design*, 2nd ed., AIAA Education Series, AIAA, Reston, VA, 2002.

[31] Kerrebrock, J. L., *Aircraft Engines and Gas Turbines*, 2nd ed., The MIT Press, Cambridge, MA, 1992.

[32] Hill, P., and Peterson, C., *Mechanics and Thermodynamics of Propulsion*, 2nd ed., Addison-Wesley, Reading, MA, 1991.

[33] Pietrzko, S., and Hofmann, R., "Mathematical Modelling of Aircraft Noise Based on Identified Directivity Patterns," *2nd AIAA/CEAS Aeroacoustics Conference*, AIAA Paper 1996-1768, 1996, doi:10.2514/6.1996-1768.

[34] European Aviation Safety Agency (EASA), "EASA Type Certificates (TCDS)," [online database], URL: `https://www.easa.europa.eu/document-library/type-certificates` [cited March 2017].

[35] Manneville, A., Pilczer, D., and Spakovszky, Z., "Noise Reduction Assessments and Preliminary Design Implications for a Functionally-Silent Aircraft," *10th AIAA/CEAS Aeroacoustics Conference*, AIAA Paper 2004-2925, 2004, doi:10.2514/6.2004-2925.

[36] Czech, M. J., Thomas, R. H., and Elkoby, R., "Propulsion Airframe Aeroacoustic Integration Effects for a Hybrid Wing Body Aircraft Configuration," *16th AIAA/CEAS Aeroacoustics Conference*, AIAA Paper 2010-3912, 2010, doi:10.2514/6.2010-3912.

[37] Huff, D. L., "Noise Reduction Technologies for Turbofan Engines," NASA-TM-214495, 2007.

[38] International Civil Aircraft Organization (ICAO), "Report by the Second CAEP Noise Technology Independent Expert Panel: Novel Aircraft-Noise Technology Review and Medium- and Long-Term Noise Reduction Goals," Doc 10017, Montreal, 2014.

[39] Felder, J. L., Kim, H. D., and Brown, G. V., "Turboelectric Distributed Propulsion Engine Cycle Analysis for Hybrid-Wing-Body Aircraft," *47th AIAA Aerospace Sciences Meeting including The New Horizons Forum and Aerospace Exposition*, AIAA Paper 2009-1132, 2009, doi:10.2514/6.2009-1132.

[40] Hornung, M., Isikveren, A. T., Cole, M., and Sizmann, A., "Ce-Liner - Case Study for eMobility in Air Transportation," *2013 Aviation Technology, Integration, and Operations Conference*, AIAA Paper 2013-4302, 2013, doi:10.2514/6.2013-4302.